Chemistry & Biodiversity

WILEY-VCH

CHEMISTRY & BIODIVERSITY

RESEARCH ARTICLE

Design, Synthesis, Characterization and In Vitro Evaluation of Anticholinesterase and Antioxidant Activities of Thiazole–Piperazine Sulphonamide Hybrids

Kethineni Sajitha[1] | Kandrakonda Yelamanda Rao[2] | Valaparla Bala Yesu[1,3] | Remya Chandran[4] | K. V. Dileep[4] | V. V. P. C. Narayana[1] | Shaik Jeelan Basha[2,5] | Katta Vamsi[6] | Donka Suresh Babu[1] | Vatturu Murali[1] | Vylu Ganesh[1] | Amooru Gangaiah Damu[2] | Doddaga Srinivasulu[1] | N. V. V. Jyothi[1]

[1]Department of Chemistry, Sri Venkateswara University, Tirupati, Andhra Pradesh, India | [2]Bioorganic Chemistry Research Laboratory, Department of Chemistry, Yogi Vemana University, Kadapa, Andhra Pradesh, India | [3]Department of Chemistry, SGK Government Degree College, Vinukonda, Andhra Pradesh, India | [4]Laboratory for Computational and Structural Biology, Jubilee Centre for Medical Research, Jubilee Mission Medical College and Research Institute, Thrissur, Kerala, India | [5]Department of Chemistry, Santhiram Engineering College (Autonomous), Nandyal, Andhra Pradesh, India | [6]Indian Institute of Science Education and Research (IISER), Tirupati, Andhra Pradesh, India

Correspondence: N. V. V. Jyothi (nvvjyothi73@gmail.com)

Received: 16 February 2025 | **Revised:** 4 April 2025 | **Accepted:** 8 April 2025

Funding: This work was supported through a research grant UGC Letter No. F.25-1/2014-15(BSR)/7-187/2007 from UGC, New Delhi for Kethineni Sajitha and another research grant (EEQ/2017/000721) from SERB under EMEQ program, New Delhi, India. Kandrakonda Yelamanda Rao (Award no. 201920-NFST-AND-02583) would like to thank the Ministry of Tribal Welfare (Govt. of India) for providing financial support in the form of a national fellowship and scholarship for higher education for ST students (NFST). Remya Chandran gratefully acknowledges the financial support from Chief Minister's Nava Kerala Post-Doctoral Fellowship, Govt. of Kerala.

Keywords: ABTS | acetylcholinesterase | Alzheimer's disease | butyrylcholinesterase | thiazole–piperazine sulphonamides

ABSTRACT

A series of thiazole–piperazine sulphonamide hybrids (**8a–k**) were synthesized, characterized and subsequently tested on Alzheimer's disease (AD) targets, including acetylcholinesterase (AChE), butyrylcholinesterase (BChE) and the ABTS radical, to assess their effectiveness. Three of the target analogues **8c**, **8e** and **8g** exhibited augmented inhibition on AChE with IC_{50} values of 2.52 ± 0.92, 2.99 ± 0.01 and 2.14 ± 0.02 μM, respectively. These analogues also showed strong inhibition selectivity against AChE over BChE. Furthermore, the congeners **8d**, **8f**, **8h** and **8i** had remarkable ABTS radical scavenging properties as their IC_{50} values were in the range of 0.05 ± 0.07–0.99 ± 0.12 μM. A study of the kinetics of inhibition of AChE for active analogue **8g** revealed a mixed type of inhibition. From the molecular docking experiments, it was clear that the compounds **8c**, **8e** and **8g** were placed optimally within the active site of AChE by interacting with both the catalytic active site (CAS) and the peripheral anionic site (PAS) and served as evidence for mixed type of inhibition. Molecular dynamics (MD) simulations of these docked complexes indicated that the root-mean-square deviation (RMSD) of the complexes stabilized below 4 Å. Among the ligands, **8c** exhibited the highest stability, with an RMSD of 3.0 ± 0.30 Å, compared to **8e** (3.77 ± 0.38 Å) and **8g** (3.50 ± 0.52 Å) in complex with human AChE (hAChE). Furthermore, in silico ADMET prediction studies revealed that the targeted analogues satisfied all the characteristics of central nervous system (CNS) acting drugs. Finally, these active compounds are determined to be nontoxic and highly neuroprotective against H_2O_2-induced cell death in SK-N-SH cell lines. These results inferred that the thiazole–piperazine sulphonamide derivatives have the potential to serve as a valuable molecular template for further in vitro and in vivo assessments in the context of the development of anti-AD agents.

1 | Introduction

Alzheimer's disease (AD), a prevailing type of dementia, is a multifactorial, chronic, progressive and eventually fatal neurodegenerative disorder. The typical clinical features are characterized by severe decline in cognitive functionality, difficulties with language, deterioration of memory, accompanied with depressive symptoms and ultimately death [1]. The current global prevalence of AD is around 55 million individuals. However, due to the rapid ageing process, this figure is projected to over 150 million by 2050; consequently AD ranks as the sixth leading cause of mortality [2]. As AD has no cure with current medications, AD is still pandemic in the 21st century, thus placing great emotional and financial burdens on sufferers and their families. Therefore, the research and development pursuits for new scaffolds as possible anti-AD drugs have gained a substantial amount of attention among medicinal chemists.

The aetiology of AD remains uncertain; nevertheless, two primary neuropathological pathways, extracellular deposition of β-amyloid (Aβ) peptide and neurofibrillary tangles (NFTs) of tau protein due to hyper phosphorylation in the brain, are found to play a significant role in the pathogenesis of the disease [3, 4]. Studies have also shown other causes behind AD such as neuroinflammation, loss of cholinergic neurotransmission, oxidative stress, disturbed mitochondrial transport to synaptic terminal and dyshomeostasis of bio-metals, and hence, several hypotheses have been proposed to address AD [5–8].

Amongst them, the 'cholinergic hypothesis' has emerged as one of the most successful approaches to ameliorating the symptoms of AD, particularly those pertaining to cognitive and behavioural function. According to the cholinergic hypothesis, degeneration of cholinergic neurons results in neurotransmission loss due to progressive decline in acetylcholine (ACh) in the cerebral cortex thereby severely altering cognitive function in AD patients. The cholinesterase (ChE) enzymes, namely, acetylcholinesterase (AChE) and butyrylcholinesterase (BChE), which catalyse the hydrolysis of Ach, are causative for this phenomenon. Therefore, increasing the level of ACh in the brain through inhibiting AChE and BChE is recognized as one of the most accepted therapeutic strategies to treat AD [9–12]. As a result, ChE inhibitors, namely, Galantamine, Donepezil and Rivastigmine, are presently accessible as a set of palliative drugs against AD [13].

Besides, oxidative stress is also an area of grave concern. Overproduction of reactive oxygen species (ROS) and progressive decline of the cellular antioxidants with ageing cause oxidative stress. The excessive oxidative stress directly affects the synaptic activity and neurotransmission of neurons, leading to cognitive dysfunction [14]. Evidently, several reports inferred oxidative stress is one of the key etiological features of AD, as oxidative stress leads to abnormal cellular metabolism, which further accelerates the formation of Aβ plaques and NFTs by promoting phosphorylation of tau, ultimately resulting in neuronal deterioration in AD patients [15, 16]. Consequently, the combination of AChE/BChE inhibition and antioxidant properties represents an additional rational approach for AD management.

ChE inhibitors like donepezil generally consist of a core ring system that interacts with peripheral anionic site (PAS), a basic centre that binds to catalytic active site (CAS) and a linker such as –O–, CH_2, –CONH–, $-CONH(CH_2)_n$ that connects these two moieties (Figure 1) [17]. Presently, thiazole bearing amino and carboxylate substituents are selected as the core heteroaromatic ring system due to their extensive biological activities, including notable antimicrobial, anticancer and antimalarial effects, along with the potent inhibitory action on AChE [18–20]. This AChE inhibitory property makes thiazole scaffold particularly valuable in addressing neurodegenerative disorders associated with diminished cholinergic neurotransmitter levels. Piperazine is employed as the basic centre, lauded for its versatility in drug design and its efficacy as CNS agent due to favourable CNS permeability and neuroprotective properties [21–24]. The incorporation of acetamide ($-NHCOCH_2-$) as linker is reported to enhance the pharmacological potential of the thiazole structure, by establishing a robust connection that optimizes ChE inhibitory activity [25]. Together, the integration of thiazole as the core, piperazine as the basic centre and acetamide as the linker demonstrated as a promising class of anti-AChE agents and reported to improve therapeutic outcomes in the management of cholinergic dysfunction [26–27]. Additionally, sulphonamide derivatives are found to have a wide spectrum of pharmacological properties like antibacterial, antiviral, antimalarial, antifungal, anticancer and antidepressant, and hence, sulphonamide moiety has become an attractive motif for repurposing old medications or generating novel multi-target therapies for complex diseases other than bacterial infections, such as AD and other CNS disorders such as diabetes, psychosis, malignancies and tumours [28–30]. Strong AD-associated BChE inhibitors were also produced from sulphonamide analogues of earlier drugs [31]. Hence, piperazine sulphonamide scaffold is preferred as a basic centre in the present study, and different substituents on this moiety are used to deduce the electronic effect on the activity.

Molecular hybrids can be designed by incorporating two or more pharmacophoric scaffolds into a single entity which will gain the ability to interact with various targets [32, 33]. Therefore, this work rationally designed a series of thiazole–piperazine sulphonamide hybrids by linking a substituted thiazole unit to a variety of piperazine sulphonamide derivatives using an optimized bioactive acetamide linker hoping these novel hybrids concurrently possess AChE and BChE inhibitory and antioxidant activities on the basis of reports on individual structural units. A total of 11 hybrid compounds were synthesized, characterized and subsequently evaluated for their in vitro activities, including inhibition of AChE and BChE, as well as antioxidant capabilities. Furthermore, optimized compounds were assessed for their cytotoxicity and neuroprotectivity in SK-N-SH cells. Kinetic study on AChE inhibition together with molecular docking and dynamics simulations and in silico ADMET predictions was carried out to explore the mode of inhibition, binding of target compounds to AChE via molecular interactions, and their suitability as CNS agents, respectively.

2 | Materials and Methods

2.1 | Chemistry

All chemicals were procured from Avra, Merck, TCI and Sigma Aldrich and used without purification. All workup procedures

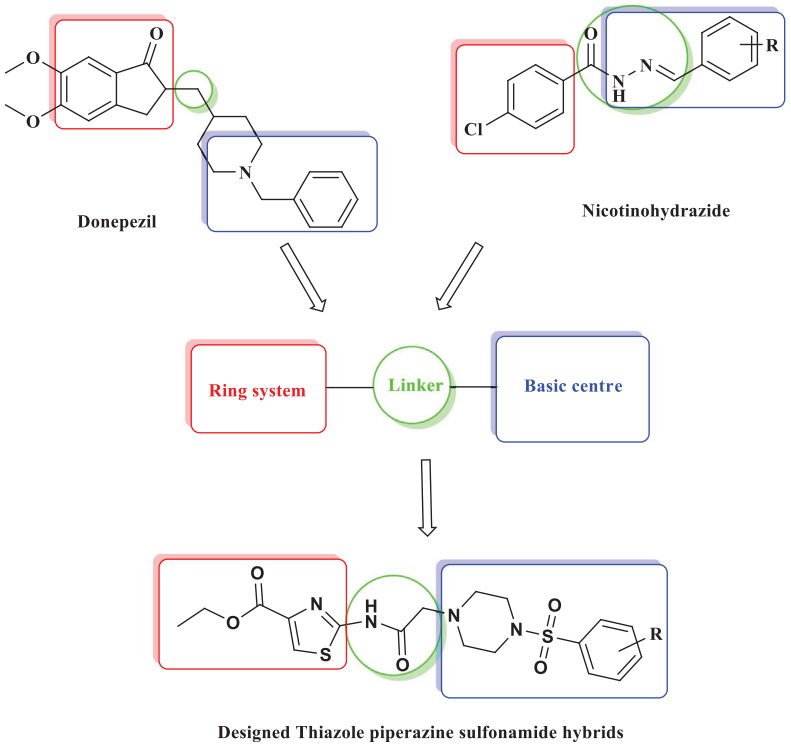

FIGURE 1 | Design of the target thiazole and piperazine sulphonamide hybrids.

and biological experiments were carried out by using double deionized water. Magnetic stirring was used to perform reactions, and TLC with 0.25 mm silica gel plates (Merck 60GF-254) and an iodine chamber or UV lamp (254 nm) visualization were utilized for monitoring all reactions. As per the requirement, substances were purified using column chromatography with silica gel (60–120 mesh). On SHIMDZU-8400 spectrometer IR spectra were collected using KBr pellet. ^{1}H NMR and ^{13}C NMR spectra were measured at 400 and 100 MHz on a Bruker spectrometer with $CDCl_3$/DMSO-d_6 solvents and TMS as an internal standard for intermediates and target compounds. Chemical shifts were expressed in units of ppm and J in Hz. The mass spectrometer Xevo TQD Quadrupole (QCA583) measured HR-MS.

2.1.1 | Synthesis of Ethyl 2-Aminothiazole-4-Carboxylate (3)

Ethyl bromopyruvate (2 g, 1 eq) and thiourea (1.17 g, 1.5 eq) were refluxed for 24 h in 100 mL of ethanol (99.9%) [34]. After completion of reaction as identified by TLC, the mixture was cooled to RT, concentrated and then poured into ice-cold water. The formed precipitate was then basified (pH 10) with 2 M NaOH and filtered. Finally, the solid was recrystallized with ethanol to produce the pure compound **3**.

2.1.2 | Synthesis of Ethyl 2-[2-Chloroacetamido] Thiazole-4-Carboxylate (4)

Thiazole amine (**3,** 1.1 g, 1 eq) and TEA (2.22 mL, 2 eq) in DCM in 15 mL were cooled to 0°C–5°C in an ice bath and stirred for 30 min [35]. Later, 2-chloroacetyl chloride (1.01 mL, 2 eq) in dry DCM (2 mL) was added slowly. Ensuring that there was no amine in the reaction mixture through TLC, the mixture was allowed to reach RT. Then the resulting liquid underwent a thorough rinsing process with water and brine. After a period of 2 h, the reaction mixture was subjected to quench using water and brine. Then the organic portion was dried with anhyd. Na_2SO_4 and the solvent were distilled off using rotavapor to yield compound **4**.

2.1.3 | Synthesis of Ethyl 2-(2-(4-(*tert*-Butoxycarbonyl) Piperazin-1-yl)Acetamido)Thiazole-4-Carboxylate (5)

A mixture of **4** (1.20 g, 1 eq), N-Boc-piperazine (1.35 g, 1.5 eq), K_2CO_3 (1.33 g, 2.0 eq), KI (0.002 g) and CH_3CN (30 mL) was refluxed at 80°C for 2 h [36]. Later, the reaction mixture was diluted with water and subsequently extracted with EtOAc (15 mL × 3). The combined organic layer was thoroughly washed with water followed by washing with satd. solution of NH_4Cl (20 mL) to remove the remaining Boc-piperazine if any and then with brine. Finally, the organic layer was dried over anhyd. Na_2SO_4 and the solvent were distilled under vacuum to get compound **5**.

2.1.4 | Synthesis of Ethyl 2-(2-(Piperazin-1-yl)Acetamido)Thiazole-4-Carboxylate (6)

Intermediate **5** (1.50 g, 1 eq) was suspended in 20 mL of methanolic HCl (10%–12% w/v) at RT and agitated magnetically for 1–2 h, continued stirring for 30 min at RT [37]. The solid formed was filtered and dissolved in 5 mL of water, and then the pH was adjusted to 8–9 using aq. Na_2CO_3 solution. The aqueous layer was subjected to liquid–liquid extraction using 20 mL of DCM.

The combined organic layers underwent a series of rinses with water (10 mL each time) till achieving a neutral pH followed by washing with brine and dried over anhyd. Na_2SO_4 and evaporated the solvent under reduced pressure to afford **6**.

2.1.5 | General Procedure for the Synthesis of Ethyl 2-(2-(4-(Phenylsulphonyl) Piperazin-1-yl)Acetamido) Thiazole-4-Carboxylates 8 (a–k)

Compound **6**, substituted benzene sulphonyl chlorides (**7a–k**) (1.20 g, 1.2 eq) and TEA (2.0 g, 2.0 eq) were dissolved in DCM (10 mL) and agitated magnetically at 40°C for 6 h [38]. The resultant mixture was extracted using DCM (30 mL), and then the organic phase was washed with brine solution (30 mL), dried over anhyd. Na_2SO_4 and concentrated. The crude substance underwent purification using column chromatography with an eluent of 5% MeOH in DCM. This process resulted in the isolation of eleven solid compounds (**8a–k**) with yields ranging from 70% to 85%.

2.1.5.1 | Ethyl 2-(2-(4-((4-Methoxyphenyl)Sulphonyl)Piperazin-1-yl)Aacetamido)Thiazole-4 Carboxylate (8a). Off white solid; yield: 84%; mp: 140°C–142°C; IR (KBr, υ_{max} cm^{-1}): 3213 (N—H), 3043 (C—H), 1755 (ester C = O), 1694 (amide C = O), 1656 (C = N), 1593 (C = C), 1365 (S = O asym.), 1262 (C—S), 1218 (C—O), 1155 (S = O sym.), 1099 (C—N), 1017, 933, 803; ^{1}H-NMR (400 MHz, $CDCl_3$) δ: 10.12 (s, 1H, 10-NH), 7.75 (s, 1H, 5-H), 7.64–7.46 (m, 2H, 2′,6′-H), 7.20–7.01 (m, 2H, 3′,5′-H), 4.39 (q, J = 8.0 Hz, 2H, 8-H), 3.85 (s, 3H, –OCH_3), 3.15–3.11 (m, 4H, 14,17-H), 3.29 (s, 2H, 12-H), 2.73–2.71 (m, 4H, 15,18-H), 1.39 (t, J = 8.0 Hz, 3H, 9-CH_3); ^{13}C-NMR (100 MHz, $CDCl_3$) δ: 167.36 (C-6), 162.46 (C-11), 160.36 (C-4′), 156.07 (C-2), 140.68 (C-4), 132.80 (C-1′), 128.90 (C-2′,6′), 121.44 (C-3′,5′), 113.61 (C-5), 67.13 (C-12), 60.48 (C-8), 54.60 (–OCH_3), 51.76 (C-14,17), 44.89 (C-15,18), 13.34 (CH_3-9); HRMS (m/z): 469.5374 $[M + H]^+$; Calcd. M.Wt: 468.5421 for $C_{19}H_{24}N_4O_6S_2$.

2.1.5.2 | Ethyl 2-(2-(4-(Phenylsulphonyl)Piperazin-1-yl)Acetamido)Thiazole-4-Carboxylate (8b). Brown solid; yield 87%; mp: 219°C–223°C; IR (KBr, υ_{max} cm^{-1}): 3263 (N—H), 2943 (C—H), 1728 (ester C = O), 1686 (amide C = O), 1654 (C = N), 1577 (C = C), 1369 (S = O asym.), 1265 (C—S), 1220 (C—O), 1114 (S = O sym.), 1099, 1017, 933, 803; ^{1}H-NMR (400 MHz, $CDCl_3$) δ: ^{1}H-NMR (400 MHz, $CDCl_3$) δ: 10.17 (s, 1H, 10-NH), 7.78 (s, 1H, 5-H), 7.68–7.62 (m, 2H, 2′,6′-H), 7.24–7.10 (m, 3H, 4′,3′,5′-H), 4.23 (q, J = 8.0 Hz, 2H, 8-H), 3.36 (s, 2H, 12-H), 3.16–3.12 (m, 4H, 14,17-H), 2.93–2.90 (m, 4H, 15,18-H), 1.33 (t, J = 8.0 Hz, 3H, 9-CH_3); ^{13}C-NMR (100 MHz, $CDCl_3$) δ: 168.40 (C-6), 163.10 (C-11), 160.82 (C-2), 143.17 (C-4), 132.29 (C-1′), 130.80 (C-4′), 129.22 (2′,6′), 128.40 (3′,5′), 112.21 (C-5), 67.55 (C-12), 60.73 (C-8), 51.83 (C-14,17), 43.34 (C-15,18), 14.06 (CH_3-9); HRMS (m/z): 439.1104 $[M + H]^+$; Calcd. M.Wt: 438.5262 for $C_{18}H_{22}N_4O_5S_2$.

2.1.5.3 | Ethyl 2-(2-(4-((4-Fluorophenyl)Sulphonyl)Piperazin-1-yl)Acetamido)Thiazole-4-Carboxylate (8c). Off white solid; yield: 81%; mp: 170°C–173°C; IR (KBr, υ_{max} cm^{-1}): 3259 (N—H), 3005 (C—H), 1755 (ester C = O), 1697 (amide C = O), 1656 (C = N), 1550 (C = C), 1365 (S = O asym.), 1238 (C—S), 1219 (C—O), 1111 (S = O sym.), 1099 (C—F), 1017, 933, 803; ^{1}H-NMR (400 MHz, $CDCl_3$) δ: 10.17 (s, 1H, 10-NH), 7.79 (s, 1H, 5-H), 7.83–7.80 (m, 2H, 2′,6′-H), 7.33–7.29 (m, 2H, 3′,5′-H), 4.40 (q, J = 8.0 Hz, 2H, 8-H), 3.29 (s, 2H, 12-H), 3.11 (m, 4H, 14,17-H), 2.71 (m, 4H, 15,18-H), 1.39 (t, J = 8.0 Hz, 3H, 9-CH_3); ^{13}C-NMR (100 MHz, $CDCl_3$) δ: 168.16 (C-6), 164.37 (C-4′), 161.37 (C-11), 157.03 (C-2), 141.73 (C-4), 130.88 (C-1′), 130.56 (2′,6′), 128.81 (2′,6′), 113.73 (C-5), 68.16 (C-12), 60.59 (C-8), 52.73 (C-14,17), 45.84 (C-15,18), 14.36 (CH_3-9); HRMS (m/z): 457.1004 $[M + H]^+$; Calcd. M.Wt: 456.5102 for $C_{18}H_{21}FN_4O_5S_2$.

2.1.5.4 | Ethyl 2-(2-(4-((4-Chlorophenyl)Sulphonyl)Piperazin-1-yl)Acetamido)Thiazole-4-Carboxylate (8d). Brown solid; yield: 78%; mp: 167°C–169°C; IR (KBr, υ_{max} cm^{-1}): 3260 (N—H), 3001 (C—H), 1728 (ester C = O), 1678 (amide —C = O), 1658 (C = N), 1531 (C = C), 1365 (S = O asym.), 1276 (C—S), 1216 (C—O), 1158 (S = O sym.), 1053 (C—Cl), 1015, 933, 803; ^{1}H-NMR (400 MHz, $CDCl_3$) δ: 10.16 (s, 1H, 10-NH), 7.83 (s, 1H, 5-H), 7.73 (d, 2H, J = 8.0 Hz, 2′,6′-H), 7.61 (d, J = 8.0 Hz, 2H, 3′,5′-H), 4.40 (q, J = 8.0 Hz, 2H, 8-H), 3.29 (s, 2H, 12-H), 3.15–3.11 (m, 4H, 14,17-H), 2.73–2.70 (m, 4H, 15,18-H), 1.39 (t, J = 8.0 Hz, 3H, 9-CH_3); ^{13}C-NMR (100 MHz, $CDCl_3$) δ: 168.18 (C-6), 161.36 (C-11), 157.01 (C-2), 141.75 (C-4), 140.16(C-4′), 133.30 (C-1′), 129.82 (3′,5′), 129.20 (2′,6′), 122.49 (C-5), 61.55 (C-12), 60.60 (C-8), 52.71 (C-14,17), 45.84 (C-15,18), 14.37 (CH_3-9); HRMS (m/z): 473.0704 $[M + H]^+$; Calcd. M.Wt: 472.9623 for $C_{18}H_{21}ClN_4O_5S_2$.

2.1.5.5 | Ethyl 2-(2-(4-((3-Nitrophenyl)Sulphonyl)Piperazin-1-yl)Acetamido)Thiazole-4-Carboxylate (8e). Yellow solid; yield: 74%; mp: 110°C–113°C; IR (KBr, υ_{max} cm^{-1}): 3258 (N—H), 3013 (C—H), 1738 (ester C = O), 1691 (amide C = O), 1653 (C = N), 1550 (N = O asym.), 1528 (C = C), 1362 (N = O sym.), 1311 (S = O asym.), 1262 (C—S), 1218 (C—O), 1109 (S = O sym.), 1017, 933, 803; ^{1}H-NMR (400 MHz, $CDCl_3$) δ: 10.10 (s, 1H, 10-NH), 8.67–8.57 (m, 2H, 3′,5′-H), 8.24–8.11 (m, 1H, 6′-H), 7.88–7.86 (m, 1H, 2′-H), 7.81 (s, 1H, 5-H), 4.37 (q, J = 8.0 Hz, 2H, 8-H), 3.49 (s, 2H, 12-H), 3.39 (m, 4H, 14,17-H), 2.81–2.69 (m, 4H, 15,18-H), 1.29 (t, J = 8.0 Hz, 3H, 9-CH_3); ^{13}C-NMR (100 MHz, $CDCl_3$) δ: 166.06 (C-6), 162.11(C-11), 153.14 (C-2), 152.45 (C-4′), 142.06 (C-4), 134.15 (C-1′), 132.57 (3′,5′), 128.81 (2′,6′), 125.97 (C-5), 65.92 (C-12), 56.97 (C-8), 51.20 (C-14,17), 44.80 (C-15,18), 14.85 (CH_3-9); HRMS (m/z): 484.0947 $[M + H]^+$; Calcd. M.Wt: 483.5103 for $C_{18}H_{21}N_5O_7S_2$.

2.1.5.6 | Ethyl 2-(2-(4-((4-Bromophenyl)Sulphonyl)Piperazin-1-yl)Acetamido)Thiazole-4-Carboxylate (8f). Brown solid; yield: 84%; mp: 186°C–188°C; IR (KBr, υ_{max} cm^{-1}): 3224 (N—H), 2986 (C—H), 1742 (ester C = O), 1684 (amide C = O), 1651 (C = N), 1536 (C = C), 1312 (S = O asym.), 1262 (C-S), 1214 (C—O), 1150 (S = O sym.), 1069 (C—Br), 1017, 933, 803; ^{1}H-NMR (400 MHz, $CDCl_3$) δ: 12.10 (s, 1H, 10-NH), 7.93 (s, 1H, 5-H), 7.83 (d, 2H, J = 8.0 Hz, 2′,6′-H), 7.67 (d, J = 8.0 Hz, 2H, 3′,5′-H), 4.29 (q, J = 8.0 Hz, 2H, 8-H), 3.32 (s, 2H, 12-H), 3.11–3.09 (m, 4H, 14,17-H), 2.67–2.64 (m, 4H, 15,18-H), 1.33 (t, J = 8.0 Hz, 3H, 9-CH_3); ^{13}CNMR (100 MHz, $CDCl_3$) δ: 169.17 (C-6), 161.31 (C-11), 158.00 (C-2), 141.49 (C-4), 134.52 (C-4′), 132.74 (C-1′), 129.81 (3′,5′), 127.82 (2′,6′), 122.66 (C-5), 60.88 (C-12), 59.98 (C-8), 51.98 (C-14,17), 46.09 (C-15,18), 14.56 (CH_3-9); HRMS (m/z): 517.0202 $[M + H]^+$; Calcd. M.Wt: 517.4133 for $C_{18}H_{21}BrN_4O_5S_2$.

2.1.5.7 | Ethyl 2-(2-(4-Tosylpiperazin-1-yl)Acetamido) Thiazole-4-Carboxylate (8g). Off White Solid; yield: 87%; mp: 189°C–191°C; IR (KBr, υ_{max} cm^{-1}): 3216 (N—H), 2994 (C—H), 1718 (ester C = O), 1690 (amide C = O), 1648 (C = N), 1532 (C = C),

1338 (S = O asym.), 1242 (C—S), 1218 (C—O), 1123 (S = O sym.), 1099, 1017, 933, 803; ^{1}H-NMR (400 MHz, $CDCl_3$) δ: 10.16 (s, 1H, 10-NH), 7.83 (s, 1H, 5-H), 7.66 (d, J = 8.0 Hz, 2H, 2′,6′-H), 7.42 (d, J = 8.0 Hz, 2H, 3′,5′-H), 4.39 (q, J = 8.0 Hz, 2H, 8-H), 3.27 (s, 2H, 12-H), 3.10–3.07 (m, 4H, 14,17-H), 2.71–2.66 (m, 4H, 15,18-H), 2.50 (s, 3H, 4′-CH_3), 1.38 (t, J = 8.0 Hz, 3H, 9-CH_3); ^{13}C-NMR (100 MHz, $CDCl_3$) δ: 167.32 (C-6), 160.35 (C-11), 156.05 (C-2), 143.26 (C-4), 140.68 (C-1′), 130.61 (C-4′), 129.87 (3′,5′), 126.80 (2′,6′), 121.45 (C-5), 67.13 (C-12), 59.62 (C-8), 51.77 (C-14,17), 44.90 (C-15,18), 20.67 (4′-CH_3), 13.34 (CH_3-9); HRMS (m/z): 453.1253 $[M + H]^+$; Calcd. M.Wt: 452.5442 for $C_{19}H_{24}N_4O_5S_2$.

2.1.5.8 | Ethyl 2-(2-(4-((4-(Trifluoromethyl)Phenyl)Sulphonyl)Piperazin-1-yl)Acetamido)Thiazole-4-Carboxylate (8h). Brown solid; yield: 79%; mp: 128°C–130°C; IR (KBr, υ_{max} cm^{-1}): 3218 (N—H), 3008 (C—H), 1729 (ester C = O), 1684 (amide C = O), 1638 (C = N), 1548 (C = C), 1322 (S = O asym.), 1262 (C—S), 1287 (C—O), 1127 (S = O sym.), 1089, 1011 (C-F), 938, 809; ^{1}H-NMR (400 MHz, $CDCl_3$) δ: 10.06 (s, 1H, 10-NH), 8.01 (d, J = 8.0 Hz, 2H, 3′,5′-H), 7.83 (m, 1H, 5-H), 7.65 (d, J = 8.0 Hz, 2H, 2′,6′-H), 4.39 (q, J = 8.0 Hz, 2H, 8-H), 3.31 (s, 2H, 12-H), 3.21–3.17 (m, 4H, 14,17-H), 2.74–2.72 (m, 4H, 15,18-H), 1.36 (t, J = 8.0, 3H, 9-CH_3); ^{13}C-NMR (100 MHz, $CDCl_3$) δ: 168.10 (C-6), 161.36 (C-11), 157.03 (C-2), 141.73 (C-4), 141.18 (C-1′), 138.76 (C-4′), 128.31 (2′,6′), 126.52 (3′,5′), 125.39 (4′-CF_3), 122.51 (C-5), 61.56 (C-12), 60.53 (C-8), 52.69 (C-14,17), 45.79 (C-15,18), 14.33 (CH_3-9); HRMS (m/z): 507.0970 $[M + H]^+$; Calcd. M.Wt: 506.5204 for $C_{19}H_{21}F_3N_4O_5S_2$.

2.1.5.9 | Ethyl 2-(2-(4-((4-Nitrophenyl)Sulphonyl)Piperazin-1-yl)Acetamido)Thiazole-4-Carboxylate (8i). Yellow solid; yield: 79%; mp: 152°C–154°C; IR (KBr, υ_{max} cm^{-1}): 3249 (N—H), 2963 (C—H), 1748 (ester C = O), 1699 (amide C = O), 1650 (C = N), 1545 (N = O asym.), 1516 (C = C), 1350 (N = O sym.), 1324 (S = O asym.), 1272 (C—S), 1218 (C—O), 1184 (S = O sym.), 1089, 1015, 930, 806; ^{1}H-NMR (400 MHz, $CDCl_3$) δ: 11.99 (s, 1H, 10-NH), 8.46 (d, J = 8.0 Hz, 2H, 3′,5′-H), 8.09 (s, 1H, 5-H), 8.02 (d, J = 8.0 Hz, 2H, 2′,6′-H), 4.29 (q, J = 7.2 Hz, 2H, 8-H), 3.35 (s, 2H, 12-H), 3.18–3.11 (m, 4H, 14,17-H), 2.73–2.68 (m, 4H, 15,18-H), 1.33 (t, J = 8.0 Hz, 3H, 9-CH_3); ^{13}C-NMR (100 MHz, $CDCl_3$) δ: 168.05 (C-6), 160.42 (C-11), 157.03 (C-2), 149.56 (C-4′), 146.97 (C-4), 140.66 (C-1′), 128.59 (2′,6′), 126.46 (3′,5′), 123.95 (C-5), 60.03 (C-12), 59.00 (C-8), 51.09 (C-14,17), 45.18 (C-15,18), 13.67 (CH_3-9); HRMS (m/z): 484.0952 $[M + H]^+$; Calcd. M.Wt: 483.5155 for $C_{18}H_{21}N_5O_7S_2$.

2.1.5.10 | Ethyl 2-(2-(4-((4-(*tert*-Butyl)Phenyl)Sulphonyl)Piperazin-1-yl)Acetamido)Thiazole-4-Carboxylate (8j). Off white solid; yield: 74%; mp: 171°C–174°C; IR (KBr, υ_{max} cm^{-1}): 3264 (N—H), 3013 (C—H), 1725 (ester C = O), 1684 (amide C = O), 1652 (C = N), 1529 (C = C), 1316 (S = O asym.), 1284 (C—S), 1218 (C—O), 1155 (S = O sym.), 1089, 1015, 937, 807; ^{1}H-NMR (400 MHz, $CDCl_3$) δ: 10.26 (s, 1H, 10-NH), 8.02 (s, 1H, 5-H), 7.85–7.81 (m, 2H, 2′,6′-H), 7.54–7.49 (m, 2H, 3′,5′-H), 4.39 (q, J = 8.0 Hz, 2H, 8-H), 3.33 (s, 2H, 12-H), 3.20-3.14 (m, 4H, 14,17-H), 2.75–2.72 (m, 4H, 15,18-H), 1.38 (s, 9H, 3xCH_3), 1.35 (t, J = 8.0 Hz, 3H, 9-CH_3); ^{13}C-NMR (100 MHz, $CDCl_3$) δ: 168.12 (C-6), 161.35 (C-11), 157.08 (C-2), 141.68 (C-4), 132.12 (C-4′), 127.64 (3′,5′), 126.37 (2′,6′), 122.48 (C-5), 61.50 (C-12), 60.48 (C-8), 52.66 (C-14,17), 46.30 (C-t. butyl), 45.79 (C-15,18), 14.35 (CH_3-9), 8.70 (3xCH_3); HRMS (m/z): 495.1730 $[M + H]^+$; Calcd. M.Wt: 494.6321 for $C_{22}H_{30}N_4O_5S_2$.

2.1.5.11 | Ethyl 2-(2-(4-((3-Bromophenyl)Sulphonyl)Piperazin-1-yl)Acetamido)Thiazole-4-Carboxylate (8k). Pale brown solid; yield: 84%; mp: 229°C–232°C; IR (KBr, υ_{max} cm^{-1}): 3261 (N—H), 2988 (C—H), 1739 (ester C = O), 1682 (amide C = O), 1658 (C = N), 1536 (C = C), 1324 (S = O asym.), 1282 (C—S), 1218 (C—O), 1158 (S = O sym.), 1079 (C-Br), 1015, 940, 810; ^{1}H-NMR (400 MHz, $CDCl_3$) δ: 10.26 (s, 1H, 10-NH), 8.02 (s, 1H, 5-H), 7.92 (s, 1H, 2′-H), 7.85–7.82 (m, 2H, 4′,5′-H), 7.54–7.49 (m, 1H, 6′-H), 4.39 (q, J = 8.0 Hz, 2H, -O-CH_2), 3.33 (s, 2H, 12-H), 3.19–3.13 (m, 4H, 14,17-H), 2.75–2.72 (m, 4H, 15,18-H), 1.37 (t, J = 8.0 Hz, 3H, 9-CH_3); ^{13}C-NMR (100 MHz, $CDCl_3$) δ: 168.12 (C-6), 161.35 (C-11), 157.08 (C-2), 141.68 (C-4), 136.77 (C-3′), 132.89 (C-1′), 130.98 (C-4′), 129.91 (C-2′), 129.11 (C-5′), 123.55 (C-6′), 122.48 (C-5), 61.50 (C-12), 60.48 (C-8), 52.66 (C-14,17), 46.30 (C-15,18), 14.36 (CH_3-9); HRMS (m/z): 517.0202 $[M + H]^+$; Calcd. M.Wt: 517.5431 for $C_{18}H_{21}BrN_4O_5S_2$.

2.2 | In Vitro Biological Assays

2.2.1 | ChE Inhibitory Activity Assay

Slightly revised Ellman's spectrophotometric method was used to assess ChE (AChE and BChE) inhibitory activity using EeAChE (from *Electrophorus electricus*) and EqBChE (from horse serum) [39]. Phosphate buffer solution (pH = 7.7, 200 mM) was freshly prepared for assay. Test sample solutions (1 mM) were made by dissolving target compounds in appropriate amount of dimethyl sulphoxide (DMSO) and diluted with phosphate buffer solution (pH = 7.7, 200 mM) to yield final concentration range.

In a 96-well microplate, the following were added in order 145 µL phosphate buffer solution (pH = 7.7, 200 mM), 10 µL test compounds solution, 80 µL 5,5-dithio-bis-(2-nitrobenzoic acid) (DTNB) solution (18.5 mg in 10 mL phosphate buffer solution), and 10 µL AChE or BChE solution (4 mU/mL enzyme in 10 mL phosphate buffer). To this assay mixture, added 15 µL of 1 mM ATCh or BTCh substrate and assayed after 5 min of pre-incubation at 25°C using Elisa microplate reader (Bio-Rad) at 415 nm absorbance. Galantamine was referenced using the same technique. Control tests were done with the reaction mixture without test sample. The calculation of the inhibition percentage was performed using the equation $(1\text{-}A_{bst}/A_{bsc}) \times 100$, where A_{bst} and A_{bsc} denote the absorbance values of AChE in the presence and absence of the test compounds, respectively. The IC_{50} values were determined using interpolation from linear regression analysis and are reported as the mean ± standard error of the mean (SEM) [36, 37].

2.2.2 | Kinetics Study AChE Inhibition

AChE inhibition by the most potent analogue **8g** was kinetically assessed using Ellman's method to calculate the inhibition constant K_i and understand the type of inhibition. Inhibitor, substrate, enzyme and DTNB stock solutions were prepared in phosphate buffer solution (pH 7.7). A concentration of 2, 2.5 and 3.5 µM of the most active inhibitor, 0.1, 0.2, 0.3, 0.4 and 0.5 µM of ACh iodide and a fixed AChE concentration (4 mU/mL in 10 mL phosphate buffer solution) were used in kinetic tests, and assessment was resembled with enzyme inhibition assay.

A 96-well microplate was loaded with 145 µL of 200 mM phosphate buffer solution (pH 7.7), 10 µL of test sample (2, 2.5 and 3.5 µM), 10 µL of ACh enzyme (4 U/mL) and 80 µL of DTNB and incubated in dark for 5 min at 25°C.

The enzymatic reaction was initiated by the addition of 15 µL of substrate ATCh (0.1–0.5 mM), which was then incubated for a duration of 5 min. Kinetic characterization was done spectrometrically using a Bio-Rad Elisa microplate reader at 415 nm [16, 40]. Each time, a control assay was performed without the test compound. Lineweaver–Burk plots were created using GraphPad Prism 8. The slopes and intercepts of the double reciprocal plots were plotted against the inhibitor concentrations in order to determine the inhibitor constants (K_{i1} and K_{i2}) associated with the binding of the inhibitor to the free enzyme and the enzyme-substrate complex as intercepts on the negative *x*-axis. Microsoft Excel was used for data analysis.

2.2.3 | ABTS Radical Scavenging Assay

The antioxidant ability of the substances was evaluated using ABTS radical scavenging assay. The ABTS radical cation, referred to as $ABTS^{*+}$, was generated by mixing equal volumes of 3 mM potassium persulphate and ABTS stock solution and placing in the dark at RT for 12–18 h. Before beginning the experiment, the work solution of $ABTS^{*+}$ was freshly made by adding methanol in a ratio of 1:29. After loading the assay mixture composed of 10 µL test solution and 290 µL $ABTS^{*+}$ work solution, the 96-well microplate was then incubated for 30 min, plate was then inserted into the Bio-Rad Elisa reader, and the absorbance was determined at 734 nm. The parallel control assay without test compound was carried out. The standard utilized was Trolox. A blank was done in each of the assays using phosphate buffer rather than test compound and Trolox. The IC_{50} values were obtained by doing each assay three times, averaging the results and reporting them as mean ± SEM [41].

2.2.4 | Cell Lines and Cultures

The SK-N-SH human neuroblastoma cells were taken from National Centre for Cell Sciences, Pune, India. The cells were cultured in MEM obtained from 0.1 mM sodium pyruvate, 0.5 mM L-glutamine and 1 mM non-essential amino acids with 10% FBS. The SK-N-SH cells were grown in 96-well plates, and plates were incubated at 37°C in a 5% CO_2 incubator.

2.2.5 | Cytotoxicity Analysis by MTT Assay

Cytotoxicity of **8c**, **8e**, **8g** and galantamine was measured by MTT assay using SK-N-SH cells as described earlier by our group [42]. Briefly, SK-N-SH cells were cultured at the amount of 0.2×10^6 cells per each well for 24 h. The compounds **8c**, **8e** and **8g** in different concentrations (30, 60 and 120 mM) were inoculated, whereas control and blank wells were also prepared with galantamine and culture media with cells, respectively. Later, the cells were incubated in 20 µL of 5 mg/mL MTT for 4 h. The DMSO (200 µL) was used to dissolve the reduced MTT formazan crystals by mixing each well through repeated pipetting. After the formation of purple colour, the absorbance was measured at 570 nm. The experiments were carried out for thrice. The blank experiment formazan was considered as 100% viability.

2.2.6 | Protection of SK-N-SH Cells From H_2O_2-Induced Cell Injury

To investigate the neuroprotective effects of synthetic compounds **8c**, **8e** and **8g** in SK-N-SH cells, the MTT assay was utilized [43, 44]. The cells (0.2×10^6 cells/well) were seeded in 96-well plates, and different concentrations (30, 60 and 120 µM) of compounds were individually added to cells and incubated for 24 h, before treatment with 1.0 mM H_2O_2. The cell viability was expressed as a relative percentage against control cultures. The positive control drug galantamine was also evaluated in the same manner for comparison. Then, 20 µL of MTT solution (5 mg/mL) was added to each well and incubated for 4 h at 37°C. Medium was removed, and formed formazan crystals were solubilized in 200 µL of DMSO and well agitated by repeated pipetting. A microplate reader was used to measure the absorbance at 570 nm, and data were plotted as per cent of control.

2.2.7 | Molecular Docking

To explore the interaction of promising compounds **8c**, **8e** and **8g** with AChE, molecular docking studies were conducted using Schrödinger Maestro (Schrödinger, LLC, New York, USA). The chemical structures of these compounds were drawn in ChemSketch and prepared using LigPrep. During preparation, the Epik program was used to generate ionized and tautomeric states of the ligands, followed by energy minimization with the Optimized Potential for Liquid Simulations (OPLS 2005) force field. The prepared ligands were then docked into the crystal structure of recombinant human AChE (hAChE) complexed with donepezil (PDB ID: 4EY7). The target protein was processed using the Protein Preparation Wizard, which included the addition of polar hydrogen atoms, optimization of hydrogen bond networks and energy minimization using the OPLS-3 force field with a root-mean-square deviation (RMSD) cut-off of 0.30 Å. The binding site was defined by generating a 20 Å grid centred on the co-crystallized ligand. Finally, the ligands were docked into the prepared grid using the extra precision (XP) docking method, and the binding free energy was estimated using the Prime MM-GBSA approach.

2.2.8 | Molecular Dynamics (MD) Simulation

To evaluate the stability and flexibility of the docked ligands within the active site of AChE, MD simulations were performed using the GPU-enabled Desmond program. Before initiating the simulations, the protein–ligand complexes were prepared using Desmond's System Builder. The protein–ligand complex was placed in an orthorhombic box with dimensions of 8 × 8 × 8 Å, containing a TIP3P explicit solvent model. To neutralize the system, eight Na^+ ions were added, along with 0.15 M NaCl to simulate physiological conditions. MD simulations were conducted using the OPLS-2005 force field for 300 ns, with trajectory record-

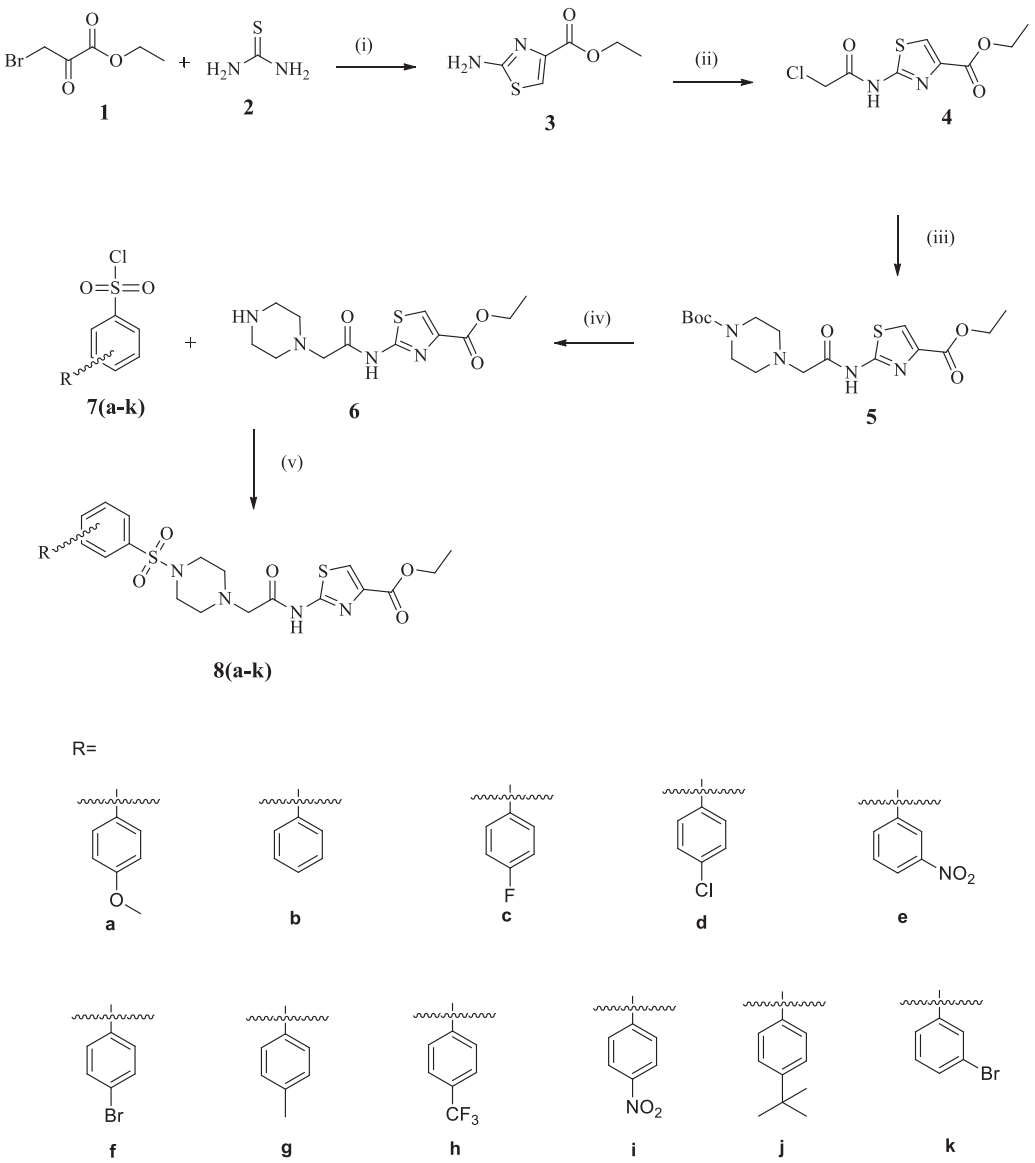

SCHEME 1 | **Reagents and conditions**: (i) EtOH, rt 24 h; (ii) chloroacetyl chloride, DCM, reflux 4–6 h; (iii) N-Boc piperazine, CH_3CN, K_2CO_3, KI; (iv) 2N HCl, CH_2Cl_2; (v) Et_3N, DCM, RT.

ing at 300 ps intervals. The NPT ensemble was applied, maintaining a constant temperature of 300 K and a pressure of 1.01 bar. The Nose–Hoover chain thermostat and Martyna–Tobias–Klein barostat were used for temperature and pressure regulation, respectively. Integration was performed using the RESPA algorithm with a 2 fs time step, whereas default settings were applied for all other parameters. Following the simulations, RMSD and root mean square fluctuation (RMSF) analyses were conducted to assess the structural stability of both the protein and ligand.

3 | Results and Discussion

3.1 | Chemistry

Scheme 1 summarizes the synthesis of thiazole–piperazine sulphonamide hybrids (**8a–k**). Initially, the synthesis of key structural motif, that is, ethyl 2-aminothiazole-4-carboxylate (**3**) was carried out by cyclization of bromopyruvate (**1**) with thiourea (**2**). Subsequently, compound **3** underwent acetylation with chloroacetyl chloride in DCM to yield compound **4** which on treatment with N-Boc-piperazine in CH_3CN, employing K_2CO_3 and KI, under reflux for 1–2 h afforded compound **5**. Compound **6** was obtained by deprotecting N-Boc group of **5** with Conc. HCl (14% w/v) at RT. Finally, intermediate **6** was coupled with the appropriate phenyl sulphonyl chlorides (**7a–k**) to furnish the final hybrid analogues **8a–k**.

3.2 | Characterization

The structures of the thiazole–piperazine sulphonamide derivatives (**8a–k**) were determined using various spectroscopic methods, including FTIR, ^{1}H NMR, ^{13}C NMR and HRMS. The FTIR spectra of compounds **8a–k** display characteristic absorption bands for N—H (3264–3213 cm^{-1}), C—H (3043–2963 cm^{-1}),

TABLE 1 | A cetylcholinesterase (AChE) and butyrylcholinesterase (BChE) inhibition and ABTS radical scavenging abilities of thiazole piperazine sulphonamide hybrids (**8a–k**), Galantamine and Trolox.

	IC_{50} (μM) ± SEM		Selectivity for	IC_{50} (μM) ± SEM
Compounds	**AChE**	**BChE**	**AChE**	**ABTS**
8a	3.56 ± 0.07	59.80 ± 1.56	16.79	2.04 ± 0.79
8b	**3.01 ± 1.20**	54.60 ± 2.24	18.14	1.52 ± 1.23
8c	**2.52 ± 0.92**	>100	—	1.38 ± 1.54
8d	3.91 ± 0.06	67.83 ± 0.76	17.35	**0.12 ± 0.87**
8e	**2.99 ± 0.01**	**40.21 ± 0.98**	13.45	2.79 ± 0.64
8f	3.24 ± 0.34	53.57 ± 1.06	16.53	**0.05 ± 0.07**
8g	**2.14 ± 0.02**	>100	—	2.93 ± 0.83
8h	3.64 ± 0.25	75.94 ± 1.66	20.86	**0.39 ± 0.21**
8i	4.47 ± 0.16	>100	—	**0.99 ± 0.12**
8j	3.85 ± 0.33	**40.69 ± 0.76**	10.57	2.09 ± 1.56
8k	3.70 ± 1.02	**35.91 ± 0.23**	9.71	**0.37 ± 0.48**
Galantamine, Trolox	0.23 ± 0.01	32.33 ± 0.46	140.57	0.70 ± 0.43

Note: Bold values indicate most active.

C = O of ester (1755–1718 cm^{-1}), C = O of amide (1699–1678 cm^{-1}), C = N (1658–1638 cm^{-1}), C = C (1593–1516 cm^{-1}), S = O (1369–1311 and 1111–1158 cm^{-1}), C–S (1284–1238 cm^{-1}), C—O (1111–1158 cm^{-1}) stretchings. In the ^1H NMR spectra, NH proton was observed as a broad peak in the range of δ 12.10–10.06, whereas aromatic protons resonate between δ 8.67 and 7.01. Thiazole proton appeared as singlet (δ 8.06–7.75); acetamide methylene protons resonated as singlet (δ 3.27–3.49). The piperazine protons are disclosed as two sets of broad peaks (δ 3.39–3.07 for sulphonamide-side protons and δ 2.93–2.64 for acetamide-side protons). The ethyl carboxylate protons found as a quartet and a triplet in the ranges of δ 4.39–4.23 and δ 1.39–1.29, respectively. The ^{13}C NMR spectra showed distinct shifts for ethyl carboxylate group (δ 168.40–167.36 for C = O; δ 60.73–56.97 for O—CH_2; δ 14.85–13.34 for –CH_3), thiazole moiety (δ 160.82–153.14; (δ 146.97–140.68; δ 125.97–112.21), acetamide group (δ 163.10–160.35; δ 68.16–60.03) and piperazine carbons (δ 52.73–51.09; δ 46.30–43.34). The carbon signals for aromatic moiety varied with the substituents. Finally, HRMS analysis further confirmed the molecular structures, as the *m/z* values of molecular ion peaks were well corroborated with the expected molecular weights of the target compounds.

3.3 | Biological Activities

3.3.1 | AChE and BChE Inhibition Activity

The multipotent characteristics of the thiazole–piperazine sulphonamide derivatives (**8a–k**) and galantamine were investigated initially by the evaluation of their inhibitory efficacies on AChE and BChE by adopting a methodology originally established by Ellman et al., but with minor modifications. Table 1 discloses the AChE and BChE inhibitory efficiencies of the titled analogues as IC_{50} values. The assessed thiazole–piperazine sulphonamide hybrid derivatives (**8a–k**) displayed varying levels of inhibitory efficacy on AChE, with IC_{50} values ranging from 2.14 ± 0.02 to 4.47 ± 0.16 μM. All the tested analogues exhibited lesser efficacy compared to the reference compound, galantamine. Markedly, compounds **8b**, **8c**, **8e** and **8g** were identified as the most potent AChE inhibitors with IC_{50} values of 3.01 ± 1.20, 2.52 ± 0.92, 2.99 ± 0.01 and 2.14 ± 0.02 μM, respectively. Amongst them, the best efficiency was attained with analogue **8g** (IC_{50} of 2.14 ± 0.02 μM) bearing 4-methyl phenyl sulphonamide moiety.

Analogues exhibited moderate to mild inhibitory effects against BChE, thereby rendering them as selective inhibitors of AChE. Among the 11 compounds tested, eight compounds exhibited inhibitory effects on BChE, with IC_{50} values ranging from 35.91 ± 0.23–75.94 ± 1.66 μM. Amongst them, **8k** with 3-bromophenyl group was identified as the most potent inhibitor of BChE as it had an IC_{50} value of 35.91 ± 0.23 μM, which is very close to that of the standard inhibitor galantamine (IC_{50} 32.33 ± 0.46 μM). Further, analogues **8e** (IC_{50} = 40.21 ± 0.98 μM) and **8j** (IC_{50} = 40.69 ± 0.76 μM) also showed significant BChE inhibitory efficacy. Majority of the active analogues demonstrated significant selectivity against AChE compared to BChE, with a selectivity index ranging from 9.71 to 20.86 μM. This selectivity is beneficial for reducing peripheral cholinergic side effects. The lack of selectivity for anti-AD drug tacrine led to its severe side effects. From these observations, an analogue **8g** with strongest anti-AChE activity was chosen for kinetic study.

3.3.2 | Kinetic Study on AChE Inhibition

Inhibition kinetics of **8g** the most active analogue against AChE was analysed in order to explore the inhibition strategy of these thiazole–piperazine sulphonamide derivatives. First, the rate of enzyme activity was assessed with various concentrations of substrate ATCh (0.1, 0.2, 0.3, 0.4 and 0.5 mM) and inhibitor **8g** (2.0, 2.5 and 3.5 μM).

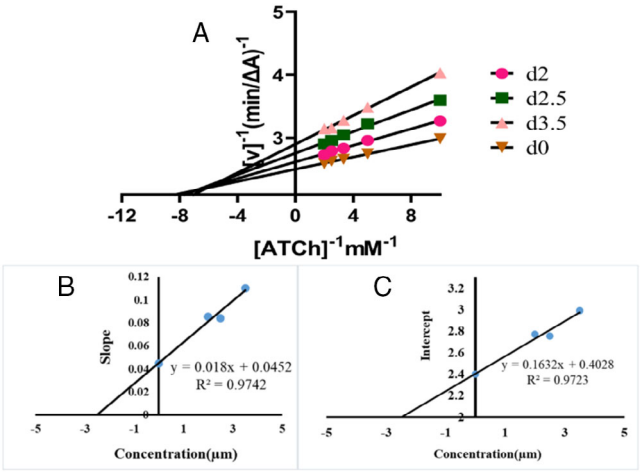

FIGURE 2 | Kinetics of AChE inhibition for compound **8g**: (A) Lineweaver–Burk plot for **8g**, (B) secondary plots of slope and various concentrations of **8g** and (C) as well as the intercept and various concentrations of **8g**.

Lineweaver–Burk plot was created using reciprocals of initial velocity and substrate concentration (1/v vs. 1/S). This double reciprocal plot disclosed a phenomenon of increasing slopes (decreased V_{max}) and intercepts (higher K_m) with increasing concentrations of **8g**. This observation is an indication of mixed-type inhibition (Figure 2). The compound **8g** exhibited inhibitory constants K_{i1} and Ki_2 of 2.51 and 2.47 μM, respectively, as estimated using secondary plots of concentration versus slope and intercept. These findings revealed that the analogue **8g** possessed the strong ability for binding with both the CAS and the PAS of AChE.

3.3.3 | Antioxidant Activity

One of the most important strategies in the development of anti-AD drugs is the reduction of oxidative stress. A well-established ABTS radical scavenging test was utilized to investigate the antioxidant power of **8a–k** and a reference drug Trolox. The antioxidant activities were reported as IC_{50} values in Table 1. The analysis of the data inferred that 11 synthesized target analogues have exceptional ABTS radical scavenging capabilities, with IC_{50} values ranging from 0.05 ± 0.075 to 2.94 ± 0.831 μM. Interestingly, some of the target compounds, namely, **8d**, **8f**, **8h** and **8k,** exhibited greater ABTS radical scavenging abilities than that of Trolox (0.70 ± 0.43 μM), a standard compound. Remarkably, variation in ABTS radical scavenging activity was noticed with varied substituents on the phenyl ring of sulphonamide part. For instance, introduction of electron-withdrawing substituents on to phenyl ring drastically improved the ABTS radical scavenging efficiency of target compounds (from **8b** to **8c**, **8i**, **8d** and **8f**) in the range of 1.1–30 folds, whereas electron-donating substituents diminished activity almost 2 times (from **8b** to **8g** and **8j**). Similarly, from **8g** to **8h** the radical scavenging activity was enhanced 7.5 times with transmission of electron-donating $-CH_3$ group to electron-withdrawing $-CF_3$ group on fourth position of phenyl group. From the activity results, it is also noted that the position of substituent on phenyl ring also played a prominent role in determining activity. For example, from 3-Br to 4-Br and from 3-NO_2 to 4-NO_2, improvement in ABTS radical scavenging activity was recorded. The active analogues **8g**, **8c**, **8e** and **8b** against AChE also had noticeable ABTS radical scavenging activity, which might be valuable feature of these new thiazole–piperazine derivatives to design multifunctional agents against AD.

3.3.4 | Cytotoxicity Against Neuroblastoma Cells

The MTT assay was performed to test the cytotoxic effects of **8c**, **8e** and **8g** and galantamine against SK-N-SH cell line [42]. In the experiment, all the compounds demonstrated over 80% cell viability at low concentration (30 μM) thereby being nontoxic to human neuroblastoma cell line.

The positive control galantamine showed 60% cell viability towards SK-N-SH cell line at final concentration of 120 μM, whereas the active analogues **8c**, **8e** and **8g** showed excellent cell viability (65%–93%) at all concentrations (Figure 3). Taken together, the compounds **8c**, **8e** and **8g** were identified as nontoxic and safe at their 50% inhibition concentrations and beyond also.

3.3.5 | Neuroprotective Effects on H_2O_2-Induced SK-N-SH Cell Injury

The neuroprotective effect of compounds **8c**, **8e**, **8g** and galantamine against H_2O_2-induced oxidative stress in SK-N-SH cells was measured by MTT assay. As shown in Figure 4, a sharp decline in cell viability to 45% was noticed after treatment of the neuronal cells with 1.0 mM H_2O_2 for 24 h, whereas compounds **8c** and **8g** showed significant protective effect in a dose-dependent manner as the cell viability increased to more than 85%. It is worthy to mention that analogue **8g** exhibited better neuroprotective ability than that of galantamine. However, analogue **8c** had the same neuroprotective capability as galantamine. Therefore, the results demonstrated that the analogues **8c**, **8e** and **8g** had excellent neuroprotective abilities against H_2O_2-induced oxidative cell injury in human neuroblastoma SK-N-SH cells.

3.4 | Molecular Docking and MD Simulation Analysis

Docking studies revealed that the ligands extend from the active site to the PAS of hAChE (Figure 5A,C,E). In these ligands, the sulphonamide region predominantly occupies the anionic site, whereas the thiazole moiety orients towards the PAS. The calculated binding energies for compounds **8C**, **8E** and **8G** were −73.34, −94.64 and −87.75 kcal/mol, respectively. MD simulations of these docked complexes indicated that the RMSD of the complexes stabilized below 4 Å (Figure 5B,D,F). Among the ligands, **8C** exhibited the highest stability, with an RMSD of 3.0 ± 0.30 Å, compared to **8E** (3.77 ± 0.38 Å) and **8G** (3.50 ± 0.52 Å) in complex with hAChE.

For compound **8c**, the fluorophenyl moiety forms a stable π–π stacking interaction with W86, persisting for 87% of the simulation time. The sulphonyl moiety establishes a hydrogen bond with G121 (72%) and an additional water-mediated hydrogen bond

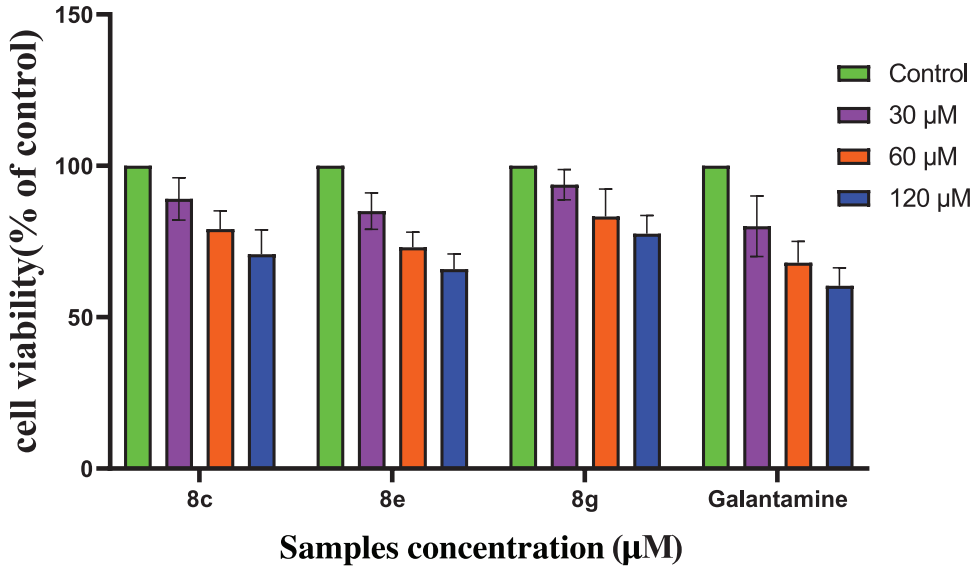

FIGURE 3 | Cytotoxic effects of **8c**, **8e**, **8g** and galantamine on SK-N-SH cell line. The values represent the mean SEM of three independent experiments in different cell batches. Statistics show neurotoxic effects of these compounds versus controls.

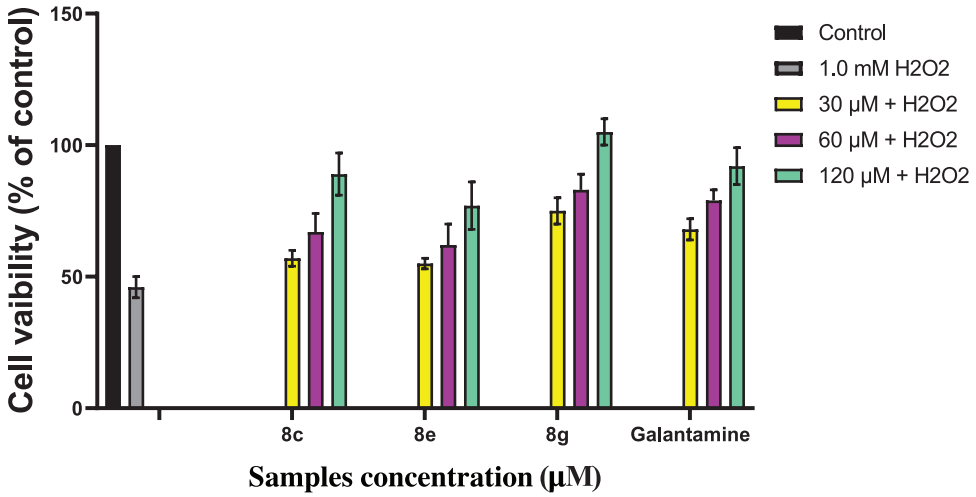

FIGURE 4 | Neuroprotective activity of analogues **8c**, **8e**, **8g** and galantamine, against H_2O_2-induced SK-N-SH cell injury.

with Glu202 and Y133 (48%), contributing to the stable binding of the compound at the bottom of the gorge. Additionally, the thiazole carboxylate moiety binds within the PAS, forming hydrogen bonds with F295 (74%) and R296 (96%) during simulation (Figure 5A,B).

In the case of compound **8e**, the nitro group orients towards Y133, forming two hydrogen bonds. The cationic nitrogen of the nitro group engages in a cation-π interaction with W86, which persists for more than 65% of the simulation time. The phenyl moiety participates in π–π stacking with H447, lasting for over 85% of the simulation time. Unlike **8c**, the sulphonyl moiety does not form direct hydrogen bonds with any residues. However, the thiazole moiety interacts with W286 through π–π stacking, and the thiazole nitrogen forms water-mediated hydrogen bonds with D74 (>60%) and transiently with Y72 (~32%). Additionally, a stable hydrogen bond with D74 (>70%) is observed via the linker NH group (Figure 5C, D).

Compound **8g**, which differs from **8C** only by the replacement of fluorine with a methyl group, exhibits slightly different interaction dynamics. The methylbenzene moiety forms a π–π stacking interaction with W86, similar to **8C** and **8E**, but with reduced stability, persisting for only 33% of the simulation time. The sulphonyl moiety forms a hydrogen bond with G121 (74%), reinforcing the complex's stability. Additionally, the keto group in the linker region forms a transient hydrogen bond with Y124. The thiazole carboxylate moiety retains hydrogen bonding interactions with F295 and R296, similar to **8C**, suggesting a conserved binding mechanism (Figure 5E, F).

3.5 | In Silico Prediction of ADMET Properties and Drug Likeness

Along with high pharmacological potency, an ideal pharmacokinetics as well as low toxicity profile is very important for a

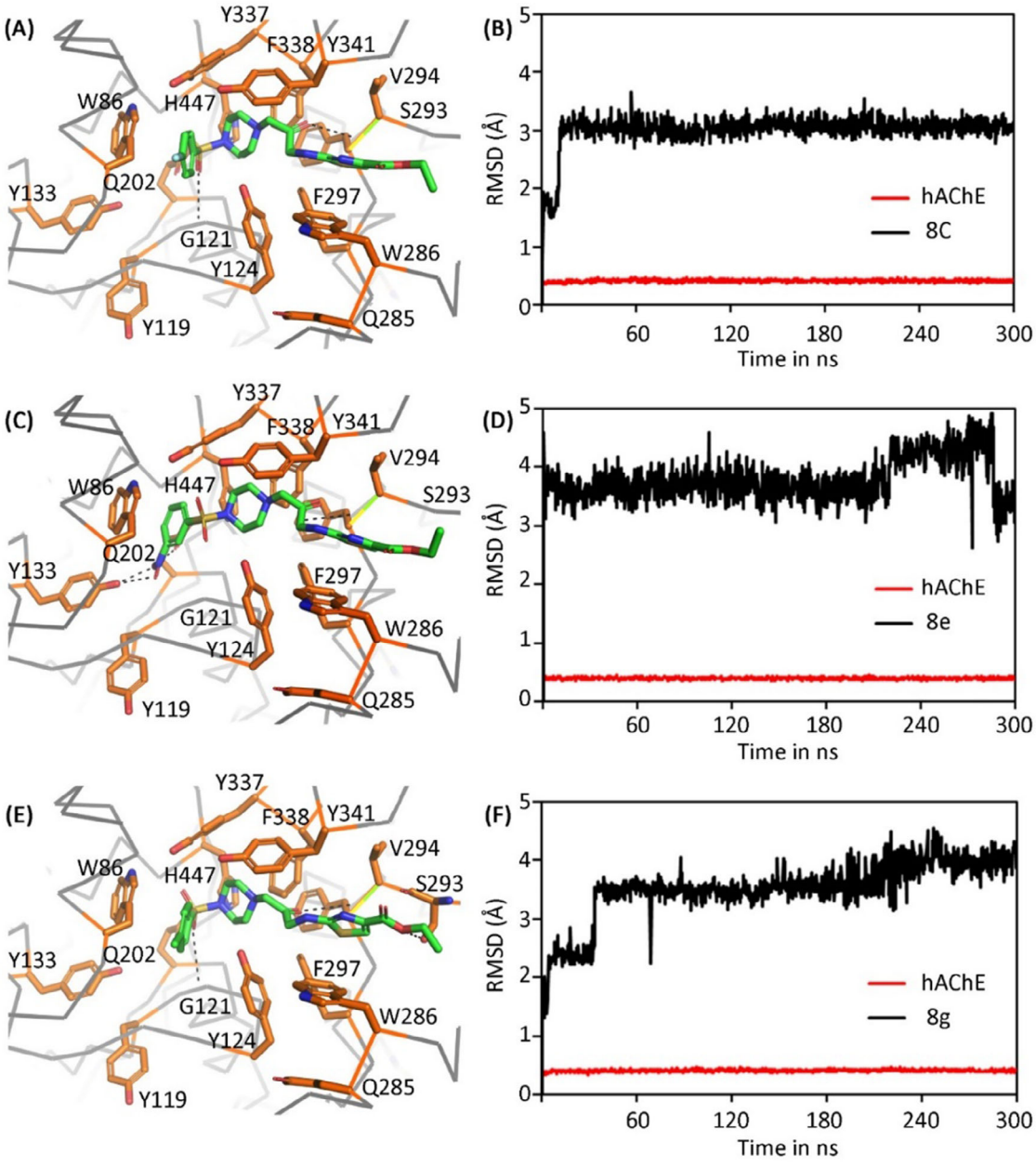

FIGURE 5 | Interactions of **8c**, **8e** and **8g** on human AChE (A, C and E); binding modes of **8c**, **8e** and **8g**, respectively, with hAChE. These ligands exhibiting partial interaction with both the active site and the peripheral anionic site of hAChE. The protein residues are represented as orange sticks and a grey ribbon, whereas ligands are depicted as green sticks. Black dashed lines indicate hydrogen bonds, partially on the active site and the peripheral anionic site of hAChE. (B, D and F) RMSD analysis of **8c**, **8e** and **8g** over a 300 ns simulation, where black lines represent ligand RMSD and red lines denote hAChE RMSD. RMSD, root-mean-square deviation.

compound to become a drug candidate. Presently, in silico studies have made the assessment of physicochemical and ADMET profiles of drug candidates extremely easy. Hence, in the present study, in silico physicochemical and ADMET properties, drug-likeness and toxicity profiles of three compounds that have multifunctional abilities against targets of AD were evaluated using ADMETlab 2.0 web tools [45].

The Lipinski's rule of five is essential for rational drug design as it predicts ideal pharmacokinetic profile of a compound. It was well demonstrated that the low permeability or poor absorption for a given compound results when it violates two of Lipinski's rule of five [46]. According to ADMETlab 2.0 web tools assessment, all the three thiazole piperazine sulphonamides (**8c**, **8e** and **8g**) tested do not violate Lipinski's rule of five demonstrating that the compounds have drug-like molecular nature. The molecules with a TPSA of 60 $Å^2$ would be well absorbed. Amongst tested, compounds **8c** and **8g** showed TPSA values near to well-absorbed range. However, according to LogP, Log S and logD values, analogues **8c**, **8e** and **8g** have optimal solubility, lipophilicity and permeability. Analysis of parameters like Caco-2-permeability, P-glycoprotein (P-gp) substrate or inhibitor and human intestinal absorption (HIA) for **8c**, **8e** and **8g** inferred that these compounds have no optimum permeability and intestinal absorption greater

than 30% [47]. The predicted values of distribution parameters like plasma protein binding (PPB), blood–brain barrier (BBB) permeability and volume of distribution (VD) indicated that the compounds **8c**, **8e** and **8g** bind to plasma proteins significantly thus have low therapeutic index. These parameters also suggested a higher distribution of **8c**, **8e** and **8g** in plasma than in tissues and ability to permeate BBB. All the tested compounds are predicted to interact with enzyme determinants CYP1A2 and CYP3A4, which makes them very suitable molecules as their probes. Safety evaluation in mammals through rat oral acute toxicity parameter indicated that these compounds are not toxic [48]. The ADME prediction results are shown in Table S1.

4 | Conclusions

In conclusion, a new series of thiazole–piperazine sulphonamide hybrids were synthesized and demonstrated to be effective multifunctional anti-AD agents with the high AChE and BChE inhibitory, antioxidant and neuroprotective properties. In this series, analogues **8b**, **8c**, **8e** and **8g** were characterized as selective, dual binding site AChE inhibitors associated with moderate antioxidant activities. Kinetic analysis inferred that the active analogues were mixed-type inhibitors that could bind to both the CAS and PAS of AChE. Hence, these analogues may have potential to regulate the Aβ aggregation process, a key pathological event of AD which warrants further study to prove it. Supportingly, molecular docking study has also proved that sulphonamide analogues bound to CAS in such a way that a portion of the molecule leaned towards the PAS of AChE. In addition, MD simulation studies confirmed that **8c**, **8e** and **8g** formed stable complexes with AChE. Further, in silico ADMET prediction studies showed that the most potent analogues are CNS active and comply with the Lipinski's rule of five. The most active compounds **8c**, **8e** and **8g** are found to be nontoxic to human neuroblastoma cells and also assessed as highly neuroprotective against H_2O_2-induced cell death in SK-N-SH cell lines. Additionally, **8d**, **8f**, **8h**, **8i** and **8k** were endowed with highly effective antioxidant characteristics as a result of their ABTS radical scavenging capabilities. All in all, these findings suggested that the thiazole–piperazine sulphonamide hybrids may be promising template for the development of novel multifunctional anti-Alzheimer's candidates and worthy to carry further in vitro and in vivo research.

Acknowledgments

This work was supported through a research grant UGC Letter No. F.25-1/2014-15(BSR)/7-187/2007 from UGC, New Delhi for Kethineni Sajitha and another research grant (EEQ/2017/000721) from SERB under EMEQ program, New Delhi, India. Kandrakonda Yelamanda Rao (Award no. 201920-NFST-AND-02583) would like to thank the Ministry of Tribal Welfare (Govt. of India) for providing financial support in the form of a national fellowship and scholarship for higher education for ST students (NFST). Remya Chandran gratefully acknowledges the financial support from Chief Minister's Nava Kerala Post-Doctoral Fellowship, Govt. of Kerala. The authors gratefully acknowledge the Laboratory for Structural Bioinformatics, RIKEN, Japan for the molecular modelling resources. The drug discovery initiative on Alzheimer's disease, Smrithi Vardhini, by the Jubilee Centre for Medical Research is gratefully acknowledged. Authors also thank Dr. R. V. J. Kashyap, Associate Professor, Department of English, Yogi Vemana University, Kadapa, for critical reading and improving the manuscript. Moreover, authors express their gratitude towards Doddaga Yashasvi Sai for her technical support.

Conflicts of Interest

The authors declare no conflicts of interest.

Data Availability Statement

The data that support the findings of this study are available in the article or in the Supporting Information of this article.

References

1. A. V. Terry and J. J. Buccafusco, "The Cholinergic Hypothesis of Age and Alzheimer's Disease-Related Cognitive Deficits: Recent Challenges and Their Implications for Novel Drug Development," *Journal of Pharmacology and Experimental Therapeutics* 306 (2003): 821–827, https://doi.org/10.1124/jpet.102.041616.

2. D. S. Auld, T. J. Kornecook, S. Bastianetto, and R. Quirion, "Alzheimer's Disease and the Basal Forebrain Cholinergic System: Relations to β-Amyloid Peptides, Cognition, and Treatment Strategies," *Progress in Neurobiology* 68 (2002): 209–245, https://doi.org/10.1016/s0301-0082(02)00079-5.

3. M. R. Farlow and J. L. Cummings, "Effective Pharmacologic Management of Alzheimer's Disease," *American Journal of Medicine* 120 (2007): 388–397, https://doi.org/10.1016/j.amjmed.2006.08.036.

4. J. Hardy and D. J. Selkoe, "The Amyloid Hypothesis of Alzheimer's Disease: Progress and Problems on the Road to Therapeutics," *Science* 297 (2002): 353–356, https://doi.org/10.1126/science.1072994.

5. L. A. Craig, N. S. Hong, and R. J. McDonald, "Revisiting the Cholinergic Hypothesis in the Development of Alzheimer's Disease," *Neuroscience and Biobehavioral Reviews* 35 (2011): 1397–1409, https://doi.org/10.1016/j.neubiorev.2011.03.001.

6. M. Bajda, A. Więckowska, M. Hebda, N. Guzior, C. A. Sotriffer, and B. Malawska, "Structure-Based Search for New Inhibitors of Cholinesterases," *International Journal of Molecular Sciences* 14 (2013): 5608–5632, https://doi.org/10.3390/ijms14035608.

7. J. M. Mason, N. Kokkoni, K. Stott, and A. J. Doig, "Design Strategies for Anti-Amyloid Agents," *Current Opinion in Structural Biology* 13 (2003): 526–532, https://doi.org/10.1016/s0959-440x(03)00100-3.

8. V. Shukla, S. Skuntz, and H. C. Pant, "Deregulated Cdk5 Activity Is Involved in Inducing Alzheimer's Disease," *Archives of Medical Research* 43 (2012): 655–662, https://doi.org/10.1016/j.arcmed.2012.10.015.

9. M. Harel, J. L. Sussman, E. Krejci, et al., "Conversion of Acetylcholinesterase to Butyrylcholinesterase: Modeling and Mutagenesis," *PNAS* 89 (1992): 10827–10831, https://doi.org/10.1073/pnas.89.22.10827.

10. L. Savini, A. Gaeta, C. Fattorusso, et al., "Specific Targeting of Acetylcholinesterase and Butyrylcholinesterase Recognition Sites. Rational Design of Novel, Selective, and Highly Potent Cholinesterase Inhibitors," *Journal of Medicinal Chemistry* 46 (2003): 1–4, https://doi.org/10.1021/jm0255668.

11. P. J. Houghton, Y. Ren, and M. J. Howes, "Acetylcholinesterase Inhibitors From Plants and Fungi," *Natural Product Reports* 23 (2006): 181–199, https://doi.org/10.1039/b508966m.

12. J. B. Shaik, D. P. Yeggoni, Y. R. Kandrakonda, et al., "Synthesis and Biological Evaluation of Flavone-8-Acrylamide Derivatives as Potential Multi-Target-Directed Anti Alzheimer Agents and Investigation of Binding Mechanism With Acetylcholinesterase," *Bioorganic Chemistry* 88 (2019): 102960, https://doi.org/10.1016/j.bioorg.2019.102960.

13. B. Penke, M. Szűcs, and F. Bogár, "New Pathways Identify Novel Drug Targets for the Prevention and Treatment of Alzheimer's Disease," *International Journal of Molecular Sciences* 24 (2023): 5383, https://doi.org/10.3390/ijms24065383.

14. E. Tönnies and E. Trushina, "Oxidative Stress, Synaptic Dysfunction, and Alzheimer's Disease," *Journal of Alzheimer's Disease* 57 (2017): 1105–1121, https://doi.org/10.3233/JAD-161088.

15. D. X. Tan, L. C. Manchester, R. Sainz, J. C. Mayo, F. L. Alvares, and R. J. Reiter, "Antioxidant Strategies in Protection Against Neurodegenerative Disorders," *Expert Opinion on Therapeutic Patents* 13 (2003): 1513–1543, https://doi.org/10.1517/13543776.13.10.1513.

16. K. Yelamanda Rao, S. Jeelan Basha, K. Monika, et al., "Development of Quinazolinone and Vanillin Acrylamide Hybrids as Multi-Target Directed Ligands Against Alzheimer's Disease and Mechanistic Insights Into Their Binding With Acetylcholinesterase," *Journal of Biomolecular Structure & Dynamics* 41 (2023): 11148–11165, https://doi.org/10.1080/07391102.2023.2203255.

17. L. Yurttaş, Z. A. Kaplancıklı, and Y. Özkay, "Design, Synthesis and Evaluation of New Thiazole-Piperazines as Acetylcholinesterase Inhibitors," *Enzyme Inhibition and Medicinal Chemistry* 28 (2012): 1040–1047, https://doi.org/10.3109/14756366.2012.709242.

18. B. N. Sağlık, D. Osmaniye, U. Acar Çevik, et al., "Design, Synthesis, and Structure—Activity Relationships of Thiazole Analogs as Anticholinesterase Agents for Alzheimer's Disease," *Molecules* 25 (2020): 4312, https://doi.org/10.3390/molecules25184312.

19. G. Turan-Zitouni, A. Ozdemir, Z. A. Kaplancikli, M. D. Altintop, H. E. Temel, and G. A. Çiftçi, "Synthesis and Biological Evaluation of some Thiazole Derivatives as New Cholinesterase Inhibitors," *Journal of Enzyme Inhibition and Medicinal Chemistry* 28 (2012): 509–514, https://doi.org/10.3109/14756366.2011.653355.

20. A. Y. Hemaida, G. S. Hassan, A. R. Maarouf, J. Joubert, and A. A. El-Emam, "Synthesis and Biological Evaluation of Thiazole-Based Derivatives as Potential Acetylcholinesterase Inhibitors," *ACS Omega* 6 (2021): 19202–19211, https://doi.org/10.1021/acsomega.1c02549.

21. M. Shaquiquzzaman, G. Verma, A. Marella, et al., "Piperazine Scaffold: A Remarkable Tool in Generation of Diverse Pharmacological Agents," *European Journal of Medicinal Chemistry* 102 (2015): 487–529, https://doi.org/10.1016/j.ejmech.2015.07.026.

22. P. Meena, V. Nemaysh, M. Khatri, A. Manral, P. M. Luthra, and M. Tiwari, "Synthesis, Biological Evaluation and Molecular Docking Study of Novel Piperidine and Piperazine Derivatives as Multi-Targeted Agents to Treat Alzheimer's Disease," *Bioorganic & Medicinal Chemistry* 23 (2015): 1135–1148, https://doi.org/10.1016/j.bmc.2014.12.057.

23. P. Piplani and C. C. Danta, "Design and Synthesis of Newer Potential 4-(N-Acetylamino) Phenol Derived Piperazine Derivatives as Potential Cognition Enhancers," *Bioorganic Chemistry* 60 (2015): 64–73, https://doi.org/10.1016/j.bioorg.2015.04.004.

24. F. Prati, C. Bergamini, R. Fato, et al., "Novel 8-Hydroxyquinoline Derivatives as Multitarget Compounds for the Treatment of Alzheimer′s Disease," *ChemMedChem* 11 (2016): 1284–1295, https://doi.org/10.1002/cmdc.201600014.

25. Z. Q. Sun, L. X. Tu, F. J. Zhuo, and S. X. Liu, "Design and Discovery of Novel Thiazole Acetamide Derivatives as Anticholinesterase Agent for Possible Role in the Management of Alzheimer's," *Bioorganic & Medicinal Chemistry Letters* 26 (2016): 747–750, https://doi.org/10.1016/j.bmcl.2016.01.001.

26. M F. Arshad, A. Alam, A. A. Alshammari, et al., "Thiazole: A Versatile Standalone Moiety Contributing to the Development of Various Drugs and Biologically Active Agents," *Molecules* 27 (2022): 3994, https://doi.org/10.3390/molecules27133994.

27. D. Osmaniye, B. N. Sağlık, U. A. Çevik, et al., "Biodegradable Polymers for Gene Delivery," *Molecules* 24 (2019): 3744, https://doi.org/10.3390/molecules24203744.

28. S. Mutahir, J. Jończyk, M. Bajda, et al., "Novel Biphenyl Bis-Sulfonamides as Acetyl and Butyrylcholinesterase Inhibitors: Synthesis, Biological Evaluation and Molecular Modeling Studies," *Bioorganic Chemistry* 64 (2016): 13–20, https://doi.org/10.1016/j.bioorg.2015.11.002.

29. S. Riaz, I. U. Khan, M. Bajda, et al., "Pyridine Sulfonamide as a Small Key Organic Molecule for the Potential Treatment of Type-II Diabetes Mellitus and Alzheimer's Disease: In Vitro Studies Against Yeast α-Glucosidase, Acetylcholinesterase and Butyrylcholinesterase," *Bioorganic Chemistry* 63 (2015): 64–71, https://doi.org/10.1016/j.bioorg.2015.09.008.

30. P. Zajdel, A. Partyka, K. Marciniec, A. J. Bojarski, M. Pawlowski, and A. Wesolowska, "Quinoline- and Isoquinoline-Sulfonamide Analogs of Aripiprazole: Novel Antipsychotic Agents?," *Future Medicinal Chemistry* 6 (2014): 57–75, https://doi.org/10.4155/fmc.13.158.

31. U. Košak, B. Brus, D. Knez, et al., "The Magic of Crystal Structure-Based Inhibitor Optimization: Development of a Butyrylcholinesterase Inhibitor With Picomolar Affinity and In Vivo Activity," *Journal of Medicinal Chemistry* 61 (2018): 119–139, https://doi.org/10.1021/acs.jmedchem.7b01086.

32. N. S. Begüm, I. Sinem, and O. Yusuf, "Synthesis of New Donepezil Analogues and Investigation of Their Effects on Cholinesterase Enzymes," *European Journal of Medicinal Chemistry* 124 (2016): 1026–1040, https://doi.org/10.1016/j.ejmech.2016.10.042.

33. T. Fatih, N. S. Begum, O. Yusuf, A. K. Zafer, and K. K. Bedia, "Design, Synthesis, Biological Activity Evaluation and In Silico Studies of New Nicotinohydrazide Derivatives as Multi-Targeted Inhibitors for Alzheimer's Disease," *Journal of Molecular Structure* 1265 (2022): 133441, https://doi.org/10.1016/j.molstruc.2022.133441.

34. R. Kuhn and K. Dury, "Ringschlüsse Mit α, α′-Dioxymuconsäure-Estern," *Justus Liebigs Annalen Der Chemie* 571 (1951): 44–68, https://doi.org/10.1002/jlac.19515710107.

35. Z.-Q. Sun, L.-X. Tu, F.-J. Zhuo, and S.-X. Liu, "Design and Discovery of Novel Thiazole Acetamide Derivatives as Anticholinesterase Agents for Possible Role in the Management of Alzheimer's," *Bioorganic & Medicinal Chemistry Letters* 26 (2016): 747–750, https://doi.org/10.1016/j.bmcl.2016.01.001.

36. K. Yelamanda Rao, S. Jeelan Basha, K. Monika, et al., "Synthesis and Anti-Alzheimer Potential of Novel α-Amino Phosphonate Derivatives and Probing Their Molecular Interaction Mechanism With Acetylcholinesterase," *European Journal of Medicinal Chemistry* 253 (2023): 115288, https://doi.org/10.1016/j.ejmech.2023.115288.

37. D. Rajasekhar, D. Srinivasulu, C. Sridhar, G. V. N. Kumar, and P. Ramesh, "Synthesis, Spectral Characterization and Antioxidant Activity of Novel Zafirlukast Sulfonyl Derivatives," *Journal of the Chinese Chemical Society* 63 (2016): 267–274, https://doi.org/10.1002/jccs.201500143.

38. M. Vatturu, K. Y. Rao, V. B. Yesu, et al., "Synthesis and In Vitro Assessment of Anticholinesterase and Antioxidant Properties of Triazineamide Derivatives," *Future Medicinal Chemistry* 14 (2022): 1741–1753, https://doi.org/10.4155/fmc-2022-0200.

39. G. L. Ellman, K. D. Courtney, V. Andres Jr, and R. M. Featherstone, "A New and Rapid Colorimetric Determination of Acetylcholinesterase Activity," *Biochemical Pharmacology* 7 (1961): 88–95.

40. M. V. K. Reddy, K. Y. Rao, G. Anusha, et al., "In-Vitro Evaluation of Antioxidant and Anticholinesterase Activities of Novel Pyridine, Quinoxaline and s-Triazine Derivatives," *Environmental Research* 199 (2021): 111320, https://doi.org/10.1016/j.envres.2021.111320.

41. S. S. Dappula, Y. R. Kandrakonda, J. B. Shaik, et al., "Biosynthesis of Zinc Oxide Nanoparticles Using Aqueous Extract of *Andrographis alata*: Characterization, Optimization and Assessment of Their Antibacterial, Antioxidant, Antidiabetic and Anti-Alzheimer's Properties," *Journal of Molecular Structure* 1273 (2023): 134264, https://doi.org/10.1016/j.molstruc.2022.134264.

42. J. B. Shaik, Y. R. Kandrakonda, M. Kallubai, et al., "Deciphering the AChE-Binding Mechanism With Multifunctional Tricyclic Coumarin Anti-Alzheimer's Agents Using Biophysical and Bioinformatics Approaches and Evaluation of Their Modulating Effect on Amyloidogenic Peptide Assembly," *International Journal of Biological*

Macromolecules 193 (2021): 1409–1420, https://doi.org/10.1016/J.IJBIOMAC.2021.10.204.

43. V. Ramakrishna, K. Preeti Gupta, H. Oruganti Setty, and K. Anand Kondapi, "Neuroprotective Effect of Emblica Officinalis Extract Against H_2O_2 Induced DNA Damage and Repair in Neuroblastoma Cells," *Journal of Homeopathy & Ayurvedic Medicine* (2014): 1–5, http://doi.org/10.4172/2167-1206.S1-002.

44. M. Harel, D. M. Quinn, H. K. Nair, I. Silman, and J. L. Sussman, "The X-Ray Structure of a Transition State Analog Complex Reveals the Molecular Origins of the Catalytic Power and Substrate Specificity of Acetylcholinesterase," *Journal of the American Chemical Society* 118 (1996): 2340–2346, https://doi.org/10.1021/JA952232H.

45. M. Bitew, T. Desalegn, T. B. Demissie, A. Belayneh, M. Endale, and R. Eswaramoorthy, "Pharmacokinetics and Drug-Likeness of Antidiabetic Flavonoids: Molecular Docking and DFT Study," *PLoS One* 16 (2021): e0260853, https://doi.org/10.1371/journal.pone.0260853.

46. M. Pathak, H. Ojha, A. K. Tiwari, D. Sharma, M. Saini, and R. Kakkar, "Design, Synthesis and Biological Evaluation of Antimalarial Activity of New Derivatives of 2,4,6-s-Triazine," *Chemistry Central Journal* 11 (2017): 1–11, https://doi.org/10.1186/S13065-017-0362-5/TABLES/4.

47. D. E. Clark, "Rapid Calculation of Polar Molecular Surface Area and Its Application to the Prediction of Transport Phenomena. 1. Prediction of Intestinal Absorption," *Journal of Pharmaceutical Sciences* 88 (1999): 807–814, https://doi.org/10.1021/js9804011.

48. M. Y. Al-Nour, M. M. Ibrahim, and T. Elsaman, "Ellagic Acid, Kaempferol, and Quercetin From Acacia nilotica: Promising Combined Drug With Multiple Mechanisms of Action„" *Current Pharmacology Reports* 5 (2019): 255–280, https://doi.org/10.1007/s40495-019-00181-w.

Supporting Information

Additional supporting information can be found online in the Supporting Information section.